Measuring the free field acoustic impedance and absorption coefficient of sound absorbing materials with a combined particle velocity-pressure sensor

R. Lanoye,[a] G. Vermeir, and W. Lauriks
Laboratorium voor Akoestiek en Thermische fysica, Katholieke Universiteit Leuven, Celestijnenlaan 200D, BE-3001 Heverlee, Belgium

R. Kruse and V. Mellert
Institut für Physik, Carl von Ossietzky Universität Oldenburg, D-26111 Oldenburg, Germany

(Received 20 October 2005; revised 17 February 2006; accepted 19 February 2006)

Acoustic surface impedance of sound absorbing materials can be measured by several techniques such as the impedance tube for normal impedance or the Tamura method for normal and oblique surface impedance. *In situ*, the acoustic impedance is mostly measured by use of impulse methods or by applying two-microphone techniques. All these techniques are based on the determination of the sound pressure at specific locations. In this paper, the authors use a method which is based on the combined measurement of the instantaneous sound pressure and sound particle velocity. A brief description of the measurement technique and a detailed analysis of the influence of the calibration, the source type, the source height, the sound incidence angle, and the sample size are included. [DOI: 10.1121/1.2188821]

PACS number(s): 43.58.Bh, 43.20.Ye, 43.20.El [LLT] Pages: 2826–2831

I. INTRODUCTION

To model the performance of acoustic absorbing materials in practice, researchers are interested in the reflection coefficient of those materials for different angles of sound incidence. The acoustic surface impedance and the absorption coefficient of absorbing materials can be measured with the impedance tube[1] for normal sound incidence or the Tamura method[2,3] for normal and oblique incidence of sound. For *in situ* measurements, common techniques are the impulse method[4] or the two-microphone technique.[5] Allard *et al.*[6] present a method for measurements around grazing incidence *in situ*. All these techniques make use of the measurement of local sound pressure.

As mentioned before, a proven technique to determine the angle dependency of the surface impedance and the absorption coefficient is described by Tamura. In this method, sound pressure is measured in two planes parallel to the surface of interest and a two-dimensional Fourier transformation is used to calculate the angle dependent surface impedance. Thus, no assumptions about the exact nature of the wave field are made. However, a drawback of the method is the rather complicated measurement setup together with the need for large test samples and the time-consuming measurement procedure.

In this paper, a new method for determining the surface impedance and the absorption coefficient of an absorbing material in the free field is investigated. A brief description of the measurement technique and a detailed analysis of the influence of the calibration, the source type, the source height, the sound incidence angle, and the sample size is included. All time-varying quantities should obey the time dependence $e^{-i\omega t}$ with $i=\sqrt{-1}$.

II. MEASUREMENT DEVICE

A. Working principle of the particle velocity transducer

The transducer consists of two very closely spaced heated wires. The measurement principle is based on the detection of the temperature difference between these two resistive sensors.[7] A traveling acoustic wave causes a time varying heat transfer from one sensor element to the other. The subsequent temperature difference results in a time-dependent difference between both electrical resistance values, which quantifies the particle velocity in a linear matter. However, due to the effects of diffusion and heat capacity, the sensitivity of the particle velocity sensor decreases with frequency.[8] In the *p-u* measurement probe, commercially known as "Microflown," a particle velocity sensor (u) and a miniature pressure microphone (p) are placed close together. In that way, local field impedance can directly be measured. This combination was shown to be able to measure the absorption coefficient in an impedance tube accurately.[9]

B. Calibration methods

Depending on frequency, a calibration can be performed in a standing wave tube or alternatively a free field calibration can be used. The standing wave tube calibration is used for lower frequencies (100 Hz–4 kHz). The free field calibration is applicable in the frequency range 200 Hz–20 kHz.

[a]Electronic mail: reinhilde.lanoye@bwk.kuleuven.be

 0001-4966/2006/119(5)/2826/6/$22.50

1. Standing wave tube calibration

In a standing wave tube, the sound pressure at a distance x from the rigid ending is given by

$$p(x,t,\omega) = A(e^{ikx} + e^{-ikx})e^{-i\omega t} \tag{1}$$

at frequencies below the cut-off frequency.

The particle velocity at the same position is given by

$$u(x,t,\omega) = \frac{1}{i\omega\rho_0}\frac{\partial p(x,t,\omega)}{\partial x} = \frac{A}{\rho_0 c}(e^{ikx} - e^{-ikx})e^{-i\omega t}. \tag{2}$$

The calibration of the pressure and particle velocity sensor as well as their phase difference is done separately to allow for the use of the combined probe (p-u probe) not only as an impedance sensor but also for intensity and particle velocity measurements.

A reference microphone is mounted at the rigid reflecting ending of the standing wave tube with a length of 76 cm and a diameter of 4.7 cm. At the other end, a loudspeaker is placed. If the p-u probe is set at a distance l from the reflecting surface (l lies typically in the range of 50 cm in these measurements), the ratio between the pressure measured by the p-u probe and the pressure at the reflecting ending is given by

$$\frac{p_{\text{probe}}(\omega)}{p_{\text{ref}}(\omega)} = \cos(kl). \tag{3}$$

The ratio between the particle velocity measured by the p-u probe and the pressure at the reflecting ending equals

$$\frac{u_{\text{probe}}(\omega)}{p_{\text{ref}}(\omega)} = \frac{i}{\rho_0 c}\sin(kl). \tag{4}$$

To calibrate the phase difference between the particle velocity sensor and the miniature pressure microphone in the combined probe, the ratio of particle velocity and pressure is measured. Theoretically, the ratio between both at the same point in the standing wave tube is

$$\frac{u_{\text{probe}}(\omega)}{p_{\text{probe}}(\omega)} = \frac{i}{\rho_0 c}\tan(kl) \tag{5}$$

and thus, the phase difference has to be equal to

$$\text{phase}\left\{\frac{u_{\text{probe}}(\omega)}{p_{\text{probe}}(\omega)}\right\} = \pm 90^\circ. \tag{6}$$

The difference between the measured phase and the theoretical value is used for calibration of the phase.

To calculate the frequency dependent sensitivity of the pressure sensor (sens_p) and particle velocity sensor (sens_u), the measured (voltage) transfer function is multiplied by the reference microphone sensitivity and, for the particle velocity sensor, additionally with $\rho \cdot c$. Following from Eqs. (3) and (4), the local maxima of these scaled transfer functions mark the sensitivity of the sensors at the respective frequency. A spline interpolation is done to obtain calibration values for the whole frequency range. In Fig. 1, the scaled transfer function and the resulting sensitivity is shown for the particle velocity sensor.

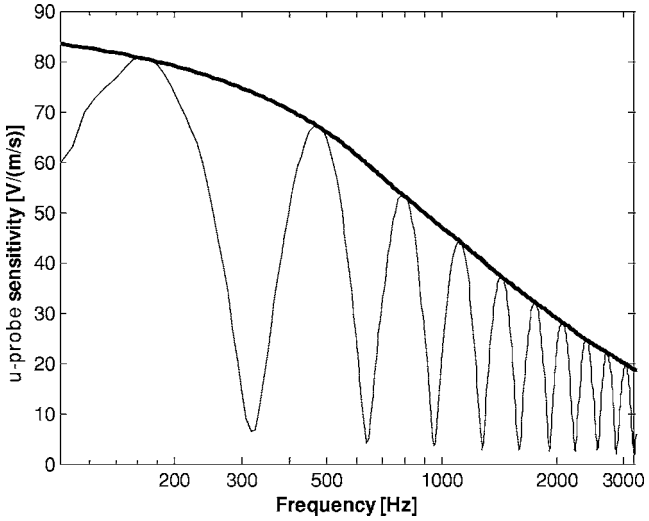

FIG. 1. Sensitivity of the Microflown element of the p-u probe. The thin line shows the measured ratio of the particle velocity at the p-u probe to the pressure at the rigid ending. The thick line marks the frequency dependent sensitivity in V/(m/s).

To obtain the phase correction function (phase_up), the local maxima and minima of the phase difference between the particle velocity sensor and the pressure microphone of the p-u probe are determined. Again, a spline interpolation is done to obtain calibration values for the whole frequency range. Following Eq. (6), the mean of the maximum and minimum values marks the deviation from ideal (zero phase) behavior and is used as correction function as shown in Fig. 2.

The preceding calibration method has the advantage of not requiring a precise value for l and c.

A correction function (CF) can be defined for the standing wave tube calibration. Later measurements have to be multiplied with this correction function to obtain calibrated measurement results. CF is defined in

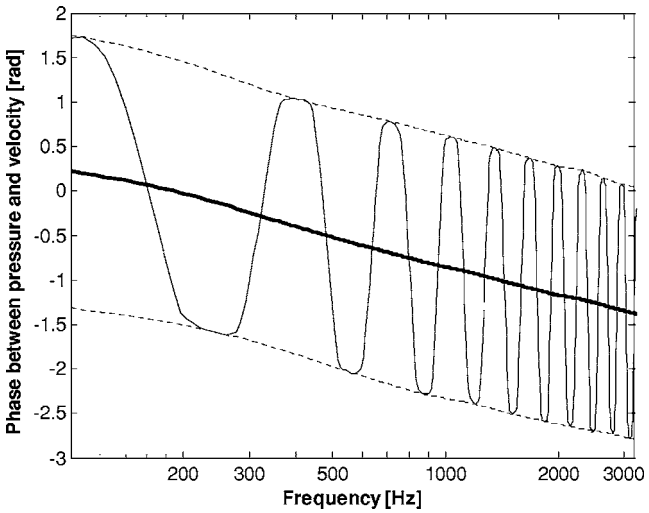

FIG. 2. Phase difference between the particle velocity sensor and the pressure element of the p-u probe. The thin line shows the measured phase between the particle velocity and the pressure at the p-u probe. The thick line marks the frequency dependent phase error.

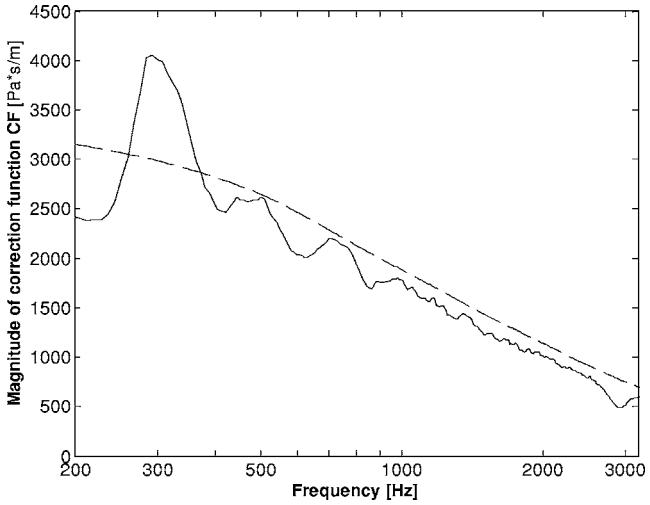

FIG. 3. Magnitude of the correction function (CF). Free field calibration (——) vs standing wave tube calibration (---).

$$\mathrm{CF} = \frac{\mathrm{sens\_}u}{\mathrm{sens\_}p} e^{i\cdot \mathrm{phase\_}up}. \tag{7}$$

Effects of damping along the tube could be shown to be negligible following an analysis based on Tijdeman's theory.[10]

2. Free field calibration

Free field calibration relies on the fact that the field impedance in a free field at a distance r is given by

$$Z_0(r,\omega) = \rho_0 c \frac{ikr}{ikr-1} \tag{8}$$

if sound is emitted by a point source.

The ratio between pressure and particle velocity is measured in free field conditions and equals Z_m. The ratio of the theoretical free field impedance to the measured impedance is the correction function,

$$\mathrm{CF} = \frac{Z_0}{Z_m}, \tag{9}$$

which is subsequently applied for calibration of all p-u measurements to obtain the calibrated field impedance. In contrast to the standing wave tube calibration, pressure and particle velocity probe cannot be calibrated separately.

The magnitude of the CF is represented in Fig. 3 for both the standing wave tube calibration [Eq. (7)] and the free field calibration [Eq. (9)]. The calibration function of the free field calibration is measured with use of a loudspeaker in a box and a probe-loudspeaker distance of 1.18 m. The probe is placed above absorbing wedges.

In the figure, a difference between both correction functions can be seen, especially at low frequencies. These deviations are due to unwanted reflections in the semi-anechoic room, e.g., coming from the floor. So, one can conclude that free field calibration is too sensitive to reflections for use at low frequencies.

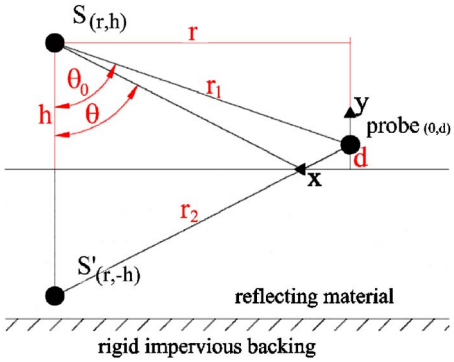

FIG. 4. (Color online) Mirror source model of the reflection of a spherical wave at an impedance plane.

III. CALCULATION TECHNIQUE

Two models are used to derive the surface impedance of a material from the measured field impedance at a certain single point above the surface. Both models assume a point source excitation of the air medium above the sample.

A. Mirror source model

This model assumes a plane-wave-like reflection. To include the reflection, a mirror source is placed behind the sample at the same distance as the physical source is placed from the sample, see Fig. 4.

This assumption is only valid if the source-sample distance is large compared to the wavelength.[11]

The angle dependent plane wave reflection coefficient $R_p(\omega,\theta)$, which can be calculated out of a measured impedance at a normal distance d above the surface, is given by

$$R_p(\omega,\theta) = e^{ik(r_1-r_2)} \frac{r_2}{r_1} \frac{Z(d,\omega)\dfrac{1-ikr_1}{-ikr_1}\cos\theta_0 - \rho_0 c}{Z(d,\omega)\dfrac{1-ikr_2}{-ikr_2}\cos\theta + \rho_0 c}. \tag{10}$$

r_1 equals the length of the direct path, r_2 is the length of the path mirror source-measurement point, and θ is the specular angle of incidence. θ_0 in this equation is the angle between the normal to the surface and the path which connects source and measurement point.

B. Asymptotic solution for locally reacting surfaces

The F-term solution of Nobile and Hayek[12] for the sound field above an impedance plane takes into account that a spherical wave is reflected differently from a plane wave. It assumes a locally reacting surface.

The velocity potential at a distance d above the impedance plane is given by

$$\phi(d) = \frac{e^{ikr_1}}{r_1} + Q\frac{e^{ikr_2}}{r_2} \tag{11}$$

in which Q denotes the spherical wave reflection coefficient

$$Q = R_p + (1-R_p)F. \tag{12}$$

R_p is the plane wave reflection coefficient, F the boundary loss function. This function F is determined by the geometry

TABLE I. Properties of the studied porous material.

Thickness (mm)	Density (kg/m^3)	Porosity (–)	Tortuosity (–)	Flow resistivity (Ns/m^4)	Viscous length (μm)	Thermal length (μm)
30	10	>0.95	1.09	10500	100	150

of the problem and the impedance of the absorbing surface. The pressure is given by

$$p(d) = \rho \frac{\partial \phi}{\partial t} = -i\rho\omega\phi, \tag{13}$$

the particle velocity by

$$u(d) = -\operatorname{grad} \phi(d). \tag{14}$$

This gradient is estimated by a finite difference approach,

$$u(d) = [\phi(d+\varepsilon) - \phi(d-\varepsilon)]/2\varepsilon \tag{15}$$

with a small ε.

With a minimum search, the surface impedance which minimizes the difference between the measured field impedance and the field impedance predicted by the model is found. The resulting surface impedance serves to calculate the plane wave absorption coefficient of the material.

If the source-sample distance and the measurement frequency are large enough, both calculation methods will be equivalent.

IV. MATERIAL DESCRIPTION

In this study, the measurement material is a 3 cm thick open-cell Melamine foam. The properties of this foam, given in Table I, are measured according to the appropriate methods. Descriptions of the methods to measure the characteristic lengths are given by Leclaire *et al.*[13] The techniques to measure porosity and tortuosity are described by Fellah *et al.*[14] The method to measure flow resistivity is given in ISO-9053.[15]

This material is assumed to behave as an equivalent fluid. To simulate the surface impedance and the absorption coefficient of this material, the theory of Johnson *et al.*[16] and Champoux and Allard[17] is used.

V. MEASUREMENT PROCEDURE

The measurements described in the following were performed in a semi-anechoic chamber with a lower limiting frequency of 150 Hz. The air in this semi-anechoic room was excited with two different sound sources, both driven with bandwith limited pseudorandom noise between 100 Hz and 6.4 kHz. The considered sound sources are a Monacor KU-156 compression driver with a 10 cm tube of $\frac{1}{2}$ in. diameter mounted on it ("point source") and a 20 cm woofer in a closed box. A Stanford Research System SR780 network analyzer was used for all measurements and postprocessing was done with MATLAB.

Samples of different sizes were placed on the rigid floor and the *p-u* probe was mounted above the surface at a height between 1.5 and 3 cm at a radial distance to the source equaling a sound incidence angle of up to 60°. The orientation of the *p-u* probe was carefully checked to agree with the normal of the sample surface.

VI. SENSITIVITY ANALYSIS

In the following, a detailed analysis of the influence of some measurement parameters is given. For the convenience of the reader and to provide a compact presentation of the results, the results are presented as absorption coefficients. Measurements are performed on a 1.8×1.2 m^2 sample, unless stated otherwise.

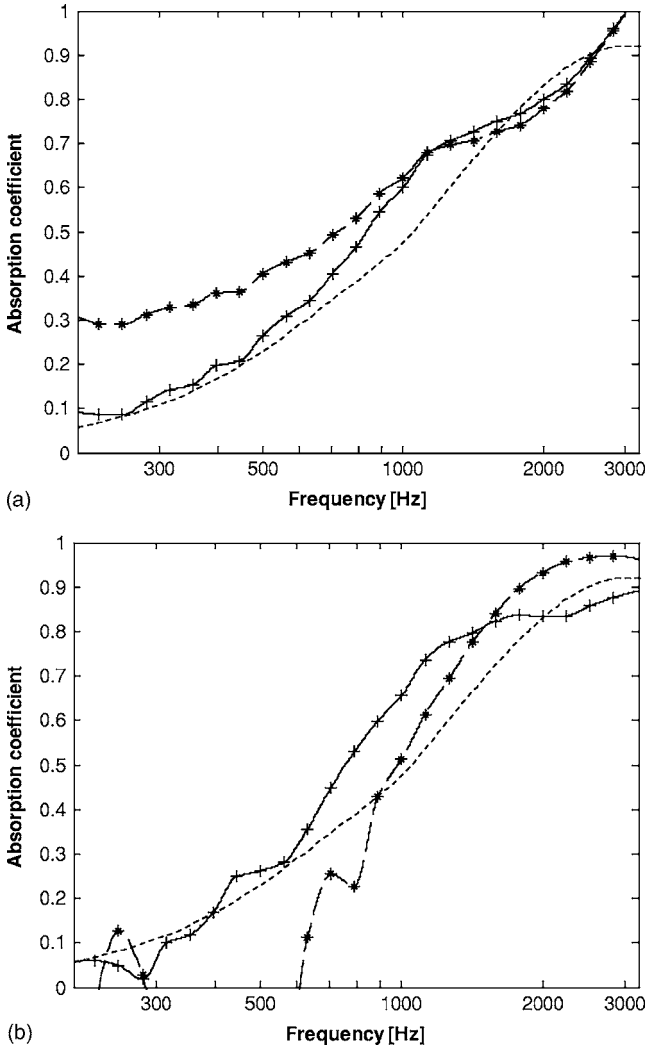

FIG. 5. Absorption coefficient of 3 cm Melamine foam for normal incidence. (a) Comparison of the mirror source model (*) and the asymptotic solution (+). Simulation results (···). (b) Comparison of the free field calibration (*) and the standing wave tube calibration (+). Simulation results (···).

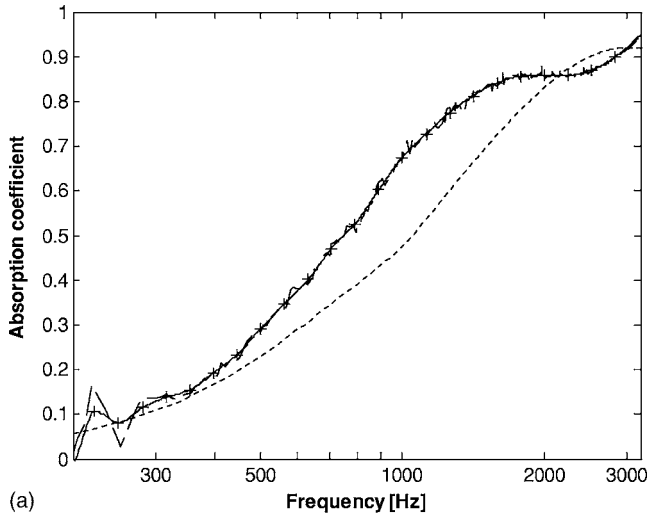

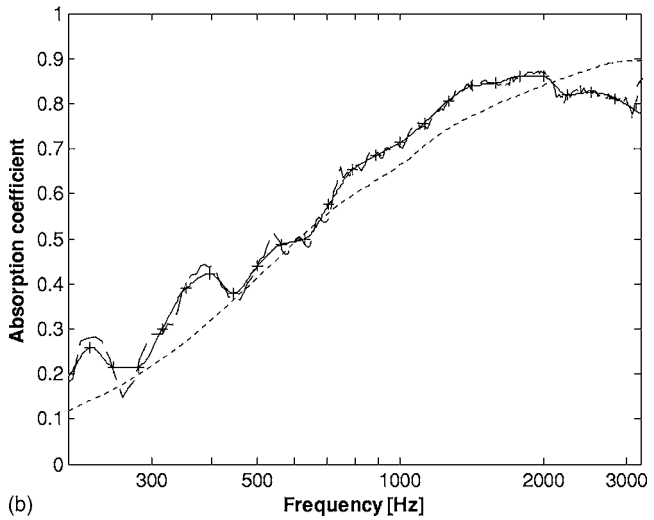

FIG. 6. Absorption coefficient of 3 cm Melamine foam. Measurement (---) with a woofer in a closed box at 1.21 m height. 1/6th octave average marked with (+). Simulation results (···). (a) Normal incidence, (b) 45° incidence.

A. Comparison of calculation models

In Fig. 5(a), a comparison is made between both above-described calculation methods. The same field impedance measurement, calibrated with a standing wave tube calibration, is used for this comparison. At low frequencies, the mirror source model differs significantly from the simulation. As shown in the experiments, the best agreement is found for the asymptotic model, which is further used as the reference.

B. Comparison of calibration methods

As can be seen in Fig. 5(b), a standing wave tube calibration allows more accurate measurements at low frequencies than a measurement with a free field calibration of the sensor probe. The surface impedance and absorption coefficient were calculated with the asymptotic solution.

C. Influence of source type

Comparison measurements were done with two different, above-described, sound sources. It could be concluded that the measurements with the loudspeaker in a box are the most accurate, especially at low frequencies, and this source will thus be used in further research. The good result for low frequencies is due to the high sound pressure that can be reached with a loudspeaker in a box. Therefore, the particle velocity at the surface of a material with high impedance is still measurable. This source has also the advantage of increasing directivity at higher frequencies and therefore avoids unwanted reflections.

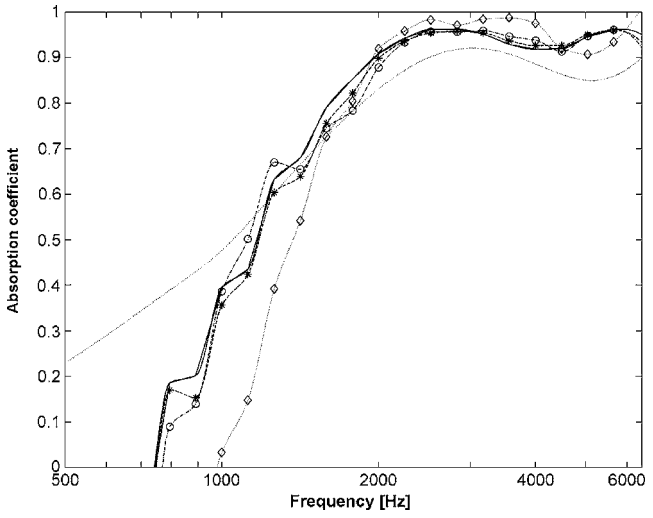

FIG. 7. Absorption coefficient of 3 cm Melamine foam for normal incidence: Influence of sample size. The size were 1.2×1.2 m^2 (---), 0.6×0.6 m^2 (*), 0.3×0.3 m^2 (°), and 0.15×0.15 m^2 ($\diamond$). Simulation results (···).

D. Influence of source height

The source was placed at different heights between 0.85 and 1.71 m above the absorbing material. If the solution of Nobile and Hayek is used to calculate the surface impedance, no significant differences can be found between the calculated absorption curves for different source heights. When the mirror source model is used, the solution below 1.2 kHz deviates more and more from the simulation when the source is placed closer to the surface.

E. Influence of incidence angle

Compared to the standing wave tube, one of the main advantages of this measurement technique is the possibility to measure the surface impedance for an arbitrary angle of sound incidence. The technique is also faster than the Tamura method. Measurements for a number of incidence angles were performed. The results for normal incidence and an angle of incidence of 45° are, respectively, shown in Figs. 6(a) and 6(b). The results for normal incidence are the best, since the phase between particle velocity and pressure is larger at normal incidence than at oblique incidence and hence the influence of the phase mismatch after calibration is smaller.

F. Influence of sample size

In this specific study, a point source was used. Knowing the required sample size is very important to know the *in situ*

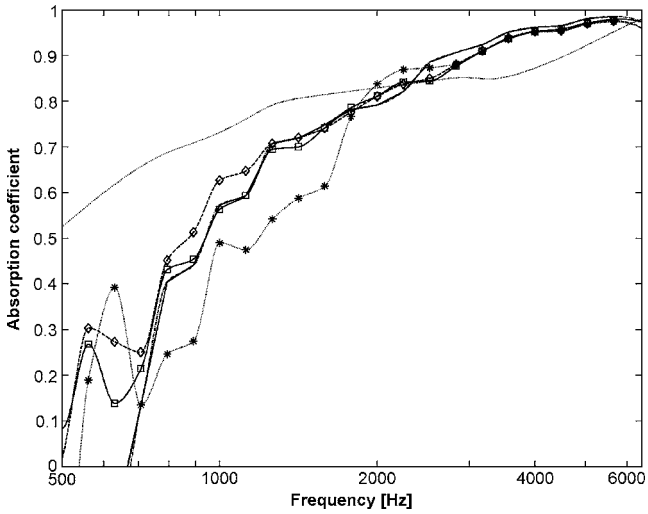

FIG. 8. Absorption coefficient of 3 cm Melamine foam for 60° incidence angle: Influence of sample size. The size were 2.4×1.2 m^2 (□), 1.8×1.2 m^2 (◇), 1.2×1.2 m^2 (---), and 0.6×0.6 m^2 (*). Simulation results (···).

applicability of the measurement device. The absorption coefficient from 200 Hz up to 6.4 kHz is measured. Results of these measurements are plotted in Figs. 7 and 8. One can clearly see that a larger sample size is necessary for more oblique angles of incidence. For 60°, there is even a sample size of 1.8×1.2 m^2 necessary to obtain good results. The poor quality of the measurements at low frequencies is due to the free field calibration, but thanks to this calibration method, one can plot higher frequency results.

VII. CONCLUSION

A new method for the measurement of the surface impedance in free field of a layer of absorbing material has been investigated in this paper. When using this method, a simultaneous measurement of the particle velocity and the pressure above the absorbing material is performed, so the field impedance close to the surface can be measured directly. The asymptotic solution for the calculation of the surface impedance has been shown to give the best results.

By means of the presented sensitivity analysis, it can be concluded that reasonably accurate and fast measurements can be performed with this new method, provided that the particle velocity-pressure transducer is adequately calibrated. Also oblique surface impedance measurements are possible with this technique. For normal to slightly oblique incidence, a rather small absorbing surface is sufficient and so the method could be applied for *in situ* analysis of local sound absorption.

ACKNOWLEDGMENT

R.L. is a Research Assistant of the Fund for Scientific Research—Flanders (Belgium).

[1]ISO 10534, "Acoustics—Determination of sound absorption coefficient and impedance in impedance tubes—, Part 1 and 2," 1998.
[2]M. Tamura, "Spatial Fourier-transform method for measuring reflection coefficients at oblique incidence. I. Theory and numerical examples," J. Acoust. Soc. Am. **88**, 2259–2264 (1990).
[3]M. Tamura, "Spatial Fourier-transform method for measuring reflection coefficients at oblique incidence. II. Experimental results," J. Acoust. Soc. Am. **97**, 2255–2262 (1995).
[4]E. Mommertz, "Angle-dependent in-situ measurement of reflection coefficients using a substraction technique," Appl. Acoust. **46**, 251–263 (1995).
[5]J. F. Allard and Y. Champoux, "In situ two-microphone technique for the measurement of the acoustic surface impedance of materials," Noise Control Eng. J. **32**, 15–23 (1989).
[6]J. F. Allard, M. Henry, V. Gareton, G. Jansens, and W. Lauriks, "Impedance measurements around grazing incidence for nonlocally reacting thin porous layers," J. Acoust. Soc. Am. **113**, 1210–1215 (2003).
[7]F. Jacobsen and H.-E. de Bree, "A comparison of two different sound intensity measurement principles," J. Acoust. Soc. Am. **118**, 1510–1517 (2005).
[8]J. W. van Honschoten, "Modelling and optimisation of the Microflown," dissertation, University of Twente, 2004.
[9]Y. Liu and F. Jacobsen, "Measurement of absorption with a *p-u* sound intensity probe in and impedance tube," J. Acoust. Soc. Am. **118**, 2117–2120 (2005).
[10]H. Tijdeman, "On the propagation of sound waves in cylindrical tubes," J. Sound Vib. **39**, 1–33 (1975).
[11]I. Rudnick, "The propagation of an acoustic wave along a boundary," J. Acoust. Soc. Am. **19**, 348–356 (1947).
[12]M. A. Nobile and S. I. Hayek, "Acoustic propagation over an impedance plane," J. Acoust. Soc. Am. **78**, 1325–1336 (1985).
[13]P. Leclaire, L. Kelders, W. Lauriks, C. Glorieux, and J. Thoen, "Determination of the viscous characteristic length in air-filled porous materials by ultrasonic attenuation measurements," J. Acoust. Soc. Am. **99**, 1944–1948 (1996).
[14]Z. E. A. Fellah, S. Berger, W. Lauriks, C. Depollier, C. Aristégui, and J.-Y. Chapelon, "Measuring the porosity and the tortuosity of porous materials via reflected waves at oblique incidence," J. Acoust. Soc. Am. **113**, 2424–2433 (2003).
[15]ISO-9053:1991, "Acoustics-materials for acoustical applications-determination of air-flow resistance."
[16]D. L. Johnson, J. Koplik, and R. Dashen, "Theory of dynamic permeability and tortuosity in fluid saturated porous media," J. Fluid Mech. **176**, 379–402 (1987).
[17]Y. Champoux and J. F. Allard, "Dynamic tortuosity and bulk modulus in air saturated porous media," J. Appl. Phys. **70**, 1975–1979 (1991).